

# Fano interference for tailoring near-field radiative heat transfer

J. E. Pérez-Rodríguez,<sup>1</sup> Giuseppe Pirruccio,<sup>1</sup> and Raúl Esquivel-Sirvent<sup>1,\*</sup>

<sup>1</sup>*Instituto de Física, Universidad Nacional Autónoma de México,  
Apartado Postal 20-364, México D.F. 01000, México*

(Dated: June 20, 2017)

We show the existence of Fano resonances in the context of near-field radiative heat transfer, which enables the strong suppression and enhancement of the spectral heat flux at specific wavelengths. We make use of the plasmon-phonon coupling in a symmetric nano cavity composed of a polaritonic material coated with a metallic layer. Each side of the cavity is kept at different temperatures. The hybridization of the plasmonic and phononic modes sustained by the multilayer structure is determined by the matching of their polarization. This leads to the opening of a thermal band gap, where heat transfer in the coupled system is inhibited for all wave vectors and for wavelengths at which the individual constituents are thermally transmissive.

Tuning and modulation of near-field radiative heat transfer (NFRHT) have recently attracted great interest due to its relevance for various technological applications such as thermal transistors [1], nanophotonic thermal devices [2], thermal diodes [3] and heat-assisted data storage [4].

Several strategies have been adopted to control the NFRHT exploiting periodic gratings [5, 6], dielectric coatings [7], graphene-coated materials [8], phase-change materials [9–11], porous materials [12–14], metamaterials [15, 16] and external magnetic fields [17]. Silicon-based meta surfaces have been shown to provide the largest radiative heat conductance [18].

Near-field radiative heat transfer is mediated by propagating and evanescent modes between two media kept at different temperatures. The former dominate when the two media are separated by a distance larger than the thermal wavelength, while the latter gives a large contribution to the total heat flux when the two media are close enough that near-field overlap takes place [19, 20]. Near field heat transfer can largely exceed the one by propagating modes only, that corresponds to the classical prediction of Stefan-Boltzman law for black bodies [21] and is a highly coherent phenomenon [22]. Several experiments have shown this anomalous heat transfer at the nanoscale [5, 23–32].

A very efficient mechanism for heat transfer is found in materials sustaining surface phonon-polaritons [33]. The enhanced heat flux found at specific wavelengths is determined by the coherent interaction of the evanescent near-fields. So far, researchers have focused on the phonon contributions to the heat flux in half spaces, single layers and multilayers [34–36]. However, the possibility of hybridization between different modes in a multilayer structure remains unexplored.

Micro- and nanocavities allow the spatial confinement of different types of excitations in the same volume. For instance, the coexistence of mechanical vibrations and optical waves in a micro resonator gave birth to the field of optomechanics [37]. Moreover, because of the ever shrinking of electronic devices, they are believed to hold

a role of primary importance in next generation electronics. An important issue is the control of the local heating and cooling, which is critical to maintaining high performances and ensure stability. The archetype structure for a cavity consists of two homogeneous, parallel and semi-infinite volumes separated by a gap and kept at different temperatures.

In nano-optics the near-field interaction has been exploited to demonstrate enhancement and suppression of optical properties of coupled systems. The coupling of a spectrally broad resonance with a narrow one leads to a distinctive phenomenon known as Fano resonance, where regions of constructive and destructive interference appear in the spectrum [38]. Fano resonances were first observed in atomic systems, and only recently an analogous mechanism has been observed in plasmonic systems, through dramatic changes in the nanostructures scattering cross section, extinction and photoluminescence of light emitters coupled to them [39–42].

In this Letter, we propose a mode hybridization scheme to tailor NFRHT. We make use of a symmetric nanocavity made of metal-coated dielectric layers, to induce a strong coupling between surface plasmon-polaritons in the metal and surface phonon-polaritons in the dielectric. This gives rise to Fano resonances which dramatically affect the spectral heat flux, eventually opening a large tailorable bandgap.

Within the fluctuating electrodynamics formalism [43], the NFRHT is described by the spectral heat flux  $S_\omega(T_1, T_2, d)$ , expressed as [13, 21]

$$S_\omega(T_1, T_2, d) = (\Theta(\omega, T_2) - \Theta(\omega, T_1)) \sum_{j=p,s} \int \frac{\beta d \beta}{(2\pi)^2} \tau_j(\omega, \beta, d), \quad (1)$$

where the sum runs over the two possible polarizations  $p$  or  $s$ ,  $\omega$  is the frequency,  $\Theta(\omega, T) = \hbar\omega \exp(\hbar\omega/k_B T) - 1)^{-1}$  is the Planck distribution function,  $\beta$  is the component of the wave vector parallel to the interfaces, related to the normal component  $\kappa$  by the relation  $\kappa^2 = (\omega/c)^2 - \beta^2$  in vacuum and  $\kappa_i^2 = (\omega/c)^2 \epsilon_i - \beta^2$  in a material with dielectric function  $\epsilon_i$ .

The energy transmission coefficient,  $\tau_j(\omega, \beta, d)$ , has two contributions, one from propagating waves ( $\beta < \omega/c$ ) and the second one from evanescent waves ( $\beta > \omega/c$ ),

$$\tau_{p,s}(\omega, \kappa, d) = \begin{cases} (1 - |r_{p,s}|^2)^2 / |1 - r_{p,s}^2 e^{2i\kappa d}|^2, & \text{if } \beta < \omega/c \\ 4\text{Im}(r_{p,s})^2 e^{-2|\kappa|d} / |1 - r_{p,s}^2 e^{-2|\kappa|d}|^2, & \text{if } \beta > \omega/c \end{cases} \quad (2)$$

where  $r_{p,s}$  are the reflectivities written in terms of the effective surface impedances [44] to account for the layered structures and the finite thickness of the slabs.

The system we consider, shown in Figure(1), is composed of two metal-coated dielectric layers separated by a gap of  $L=10$  nm. Each dielectric layer is made of a polaritonic material, NaBr, while the metallic coating is made of porous Bi. The thickness of Bi is  $d_1=75$  nm, while the thickness  $d_2$  of NaBr varies between 75 and 750 nm. The temperature difference within the cavity is 300 K, well below the Wien wavelength associated to  $T_1$  and  $T_2$ . The dielectric function of the NaBr is a Lorentz type  $\epsilon_{NaBr} = 2.6(\omega^2 - \omega_{LO}^2 + i\omega\gamma_a) / (\omega^2 - \omega_{TO}^2 + i\omega\gamma_a)$ , where  $\omega_{LO} = 39 \times 10^{12}$  rad/s is the longitudinal phonon frequency,  $\omega_{TO} = 25 \times 10^{12}$  rad/s is the transverse phonon frequency, and  $\gamma_a = 10^{-2}\omega_{TO}$  is the damping parameter [45]. For bulk Bi, we consider a Drude model with a plasma frequency of  $\omega_p = 60.77 \times 10^{12}$  rad/s, plus a sum of nine Lorentz oscillators [46]. The dielectric function of a porous Bi layer is described by a Bruggeman effective medium approximation [14] in which the resulting effective plasma frequency is given by  $\omega_{peff} = \omega_p \sqrt{(2-3f)/3}$ , where  $f$  is the porosity of the Bi [47, 48].

We first analyze the individual contributions to the NFRHT of the two NaBr layers and the two Bi layers. The left column of Fig. 2 displays the  $p$ -polarized trans-

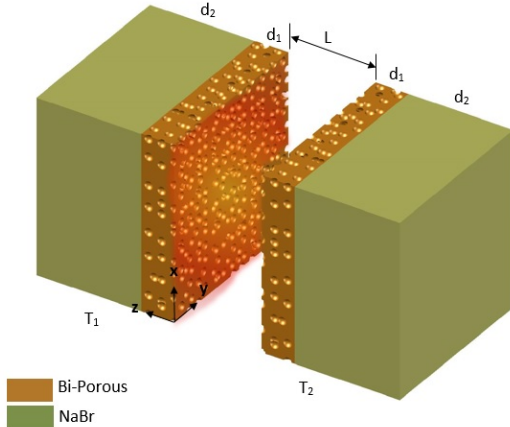


FIG. 1. Geometry of the symmetric nanocavity formed by a polaritonic material (NaBr) coated by a layer of porous Bi. The two sides of the cavity are kept at different temperature ( $T_1 = 300$  K and  $T_2 = 0$  K).

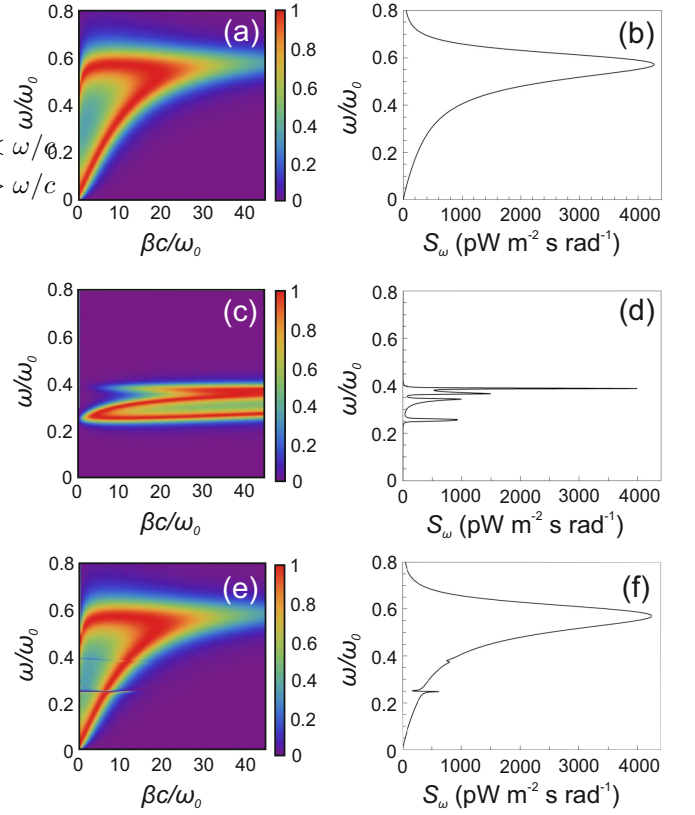


FIG. 2. (a,c,e)  $p$ -polarized transmission coefficient as a function of the normalized frequency and normalized wave vector. (b,d,e) Spectral heat flux as a function of the normalized frequency. The cavity is formed by (a,b) two 75 nm-thick, non-porous Bi layers, (c,d) two 75 nm-thick NaBr layers and (e,f) two 75 nm-thick, non-porous Bi layers and two 75 nm-thick NaBr layers.

mission coefficient,  $\tau_p$  (Eq. (2)), as a function of the normalized frequency,  $\omega/\omega_0$  with  $\omega_0 = 10^{14}$  rad/s, and normalized wave vector  $\beta c/\omega_0$ . On the right column, we show the spectral heat flux,  $S_\omega$  (Eq. (1)), as a function of the normalized frequency. Figures 2(a-b) and (c-d) correspond to the two non-porous 75 nm-thick Bi layers and the two 75 nm-thick NaBr layers, respectively. The light cone can be appreciated in panels (a,c,e) for values of the wave vector very close to 0. The dispersive and spectrally broad feature in Fig. 2(a) is associated with the excitation of the evanescent gap surface plasmon polariton (G-SPP) [49]. This mode arises from the coupling of surface plasmon polaritons sustained by the two metallic layers (see Supplemental material (SM) [50]) and for large values of  $\beta c/\omega_0$  it approaches the value  $\omega_{peff} \simeq \omega_p$ . The contribution of the G-SPP to  $S_\omega$  is shown in Fig. 2(b) which is peaked in correspondence to the dispersionless regions of  $\tau_p$ . Figure 2(c) and (d) display several sharp features corresponding to the excitation of surface phonon polaritons (SPhPs). In the bulk case, the longitudinal and the degenerate transverse optical phonon appear for  $\omega/\omega_0=0.4$

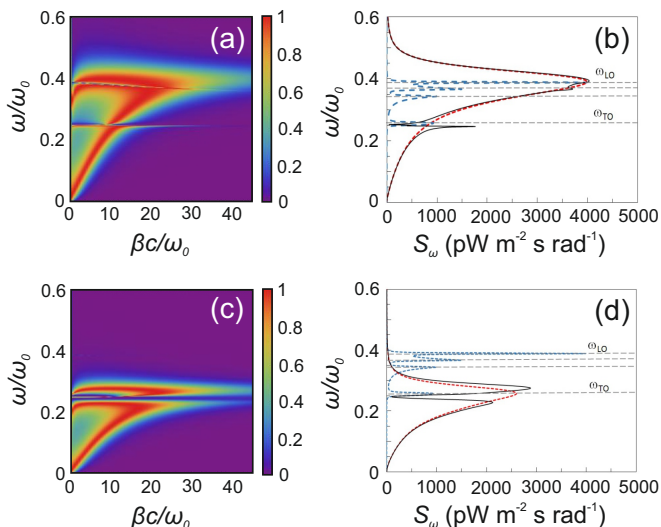


FIG. 3.  $p$ -polarized transmission coefficient as a function of the normalized frequency and normalized wave vector for the structure displayed in Fig. 1 with a Bi porosity of (a) 0.35 and (c) 0.53. Spectral heat flux as a function of the normalized frequency for the structure displayed in Fig. 1 with a Bi porosity of (b) 0.35 and (d) 0.53. The dashed red curve represents the heat flux associated to the G-SPP; the dashed blue curve represents the heat flux associated to the SPhPs; and the black continuous curve represents the total heat flux of the structure. Gray-dashed lines indicate the position of the longitudinal and transverse SPhPs.

and 0.25, respectively (see SM [50]). In contrast, multiple interfaces allows the excitation of several longitudinal and transverse modes. These sharp non-dispersive resonances appear in the same wavelength range of the dispersive G-SPP. Therefore, the NFRHT of the structure composed of the polaritonic material and the plasmonic one is expected to arise from the coupling of G-SPP and SPhPs, which we termed bare modes of the structure. In Fig. 2(e) and (f)  $\tau_p$  and  $S_\omega$  for the complete structure are shown, respectively. The small asymmetric features around  $\omega/\omega_0=0.25$  and 0.4 are due to the coupling between G-SPP and SPhPs, allowed by the longitudinal and transverse polarization components of the G-SPP, which interact with the longitudinal and transverse SPhPs, respectively. Even though a modification of  $S_\omega$  is visible for frequencies close to the phonon ones, the overall plasmon-phonon coupling is weak because of the limited spectral overlap of the bare modes of the system.

To optimize the coupling of the G-SPP and the SPhPs we vary the porosity of the Bi layer which effectively lowers its plasma frequency (see SM [50]). We assume that the porosity only affects the plasma frequency without introducing additional scattering channels for the bare modes. In Figs. 3(a) and (c) we plot  $\tau_p$  for two values of the porosity,  $f=0.35$  and 0.53, which shift  $\omega_{peff}$  to the frequencies of the longitudinal and transverse SPhPs, respectively.

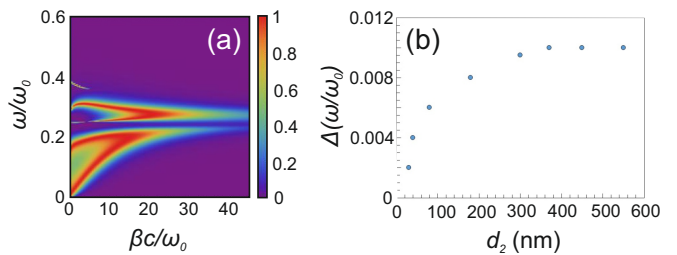


FIG. 4. (a)  $p$ -polarized transmission coefficient as a function of the normalized frequency and normalized wave vector for the structure displayed in Fig. 1 with the thickness of the NaBr layer equals to 750 nm. (b) Width of the bandgap at  $\beta c/\omega_0=18$  as a function the thickness of the NaBr layer.

In Fig. 3(a) the plasma frequency is tuned to  $\omega_{LO}$ . We observe a weak coupling between the bare modes for frequencies close to  $\omega_{LO}$ , while close to the transverse phonon frequency,  $\omega_{TO}$ , a stronger coupling appears. In order to analyze this mode coupling, in Fig. 3(b) the contributions to  $S_\omega$  from the NaBr layers and porous Bi layers are plotted with dashed blue and red curves, respectively. The black continuous curve represents  $S_\omega$  for the complete structure. The hybridization between the bare modes becomes evident close to  $\omega_{TO}$  where Fano interference occurs and  $S_\omega$  displays an asymmetric line shape. This is due to the interference between the spectrally broad G-SPP and the spectrally sharp SPhPs which allows tailoring the radiative heat transfer by creating spectral regions of enhanced and suppressed heat flux with respect to the one due to the bare modes.

By tuning the G-SPP peak to the transverse SPhP (see Figs. 3(c-d)) we obtain a spectral window where the heat transfer is forbidden for all wave vectors, although  $S_\omega$  associated to the bare modes exhibits a maximum. This phenomenon is the thermal analogy of the electromagnetically induced transparency observed in resonant photonic nanostructures [51–55]. We associate the splitting of the G-SPP band to the strong coupling between the G-SPP and the transverse SPhPs resulting in the excitation of plasmon-phonon polaritons. The contribution to the NFRHT due to the coupling of the G-SPP with the longitudinal phonons is always weak or absent due to the polarization mismatch between the bare modes. Calculation for the total  $S_\omega$  is found in the SM [50].

The spectral window of forbidden NFRHT is determined by the coupling efficiency of the G-SPP with the transverse SPhP, which, in turn, is related to the geometry of the cavity. In Fig. 4 we study the opening of the thermal bandgap for different values of the thickness,  $d_2$  of the NaBr layers and for  $f=0.53$ , while all the other geometrical parameters are kept constant. In Fig. 4(a) we plot  $\tau_p$  for  $d_2=750$  nm, while in Fig. 4(b) the width of the bandgap at  $\beta c/\omega_0=18$  is plotted as a function  $d_2$ . We see that the width of the bandgap saturates as  $d_2$  grows. This can be explained by looking at the decay length of

the electric field of the plasmon-phonon polariton, which can be estimated as [49]  $L_d \simeq |\kappa_{NaBr}|^{-1}$  and is equal to 160 nm for  $\beta c/\omega=18$ . For  $d \ll L_d$  the field leaks out the structure and, correspondingly, more phonon peaks appear in  $S_\omega$  (see Fig. 3) with respect to the bulk case (see SM [50]).

In conclusion, we demonstrated the excitation of Fano resonances and the modulation of NFRHT in a symmetric nanocavity composed of a polaritonic material coated with a metallic layer. These resonances arise from the coupling of surface plasmon polaritons and surface phonon polaritons sustained by each layer and strong suppression and enhancement of the total spectral heat flux in specific frequency regions is shown. The mode hybridization is explained in terms of polarization matching and it causes the opening of a thermal bandgap. We show that the width of the bandgap can be controlled through the geometrical parameters of the nanocavity, and that under resonant conditions, the thermal properties of the nanocavity are radically different from those of its constituents.

This work was supported by UNAM-DGAPA (PA-PIIT IA102117, IN110916), CONACYT-postdoctoral fund 291053 and PIIF-UNAM. We thank E. Y. Santiago for her suggestions and careful reading of the manuscript.

G. P. and J. E. P. R. contributed equally to this work.

---

### Supporting Information Available

\* [raul@fisica.unam.mx](mailto:raul@fisica.unam.mx)

- [1] P. Ben-Abdallah and S. Biehs, “Near-field thermal transistor,” *Phys. Rev. Lett.* **112**, 044301 (2014).
- [2] A. Lenert, D. M. Bierman, Y. Nam, W. R. Chan, I. Celanovic, M. Soljacic, and E. N. Wang, “A nanophotonic solar thermophotovoltaic device,” *Nat Nano* **9**, 126–130 (2014).
- [3] C. R. Otey, W. T. Lau, and S. Fan, “Thermal rectification through vacuum,” *Phys. Rev. Lett.* **104**, 154301 (2010).
- [4] W. A. Challener, C. Peng, A. V. Itagi, D. Karns, W. Peng, Y. Peng, X. Yang, X. Zhu, N. J. Gokemeijer, Y. T. Hsia, G. Ju, R. E. Rottmayer, M. A. Seigler, and E. C. Gage, “Heat-assisted magnetic recording by a near-field transducer with efficient optical energy transfer,” *Nat Photon* **3**, 220–224 (2009).
- [5] R. St-Gelais, B. Guha, L. Zhu, S. Fan, and M. Lipson, “Demonstration of strong near-field radiative heat transfer between integrated nanostructures,” *Nano Letters* **14**, 6971–6975 (2014).
- [6] R. Messina, A. Noto, B. Guizal, and M. Antezza, “Radiative heat transfer between metallic gratings using fourier modal method with adaptive spatial resolution,” *Phys. Rev. B* **95**, 125404 (2017).
- [7] C.J. Fu and W.C. Tan, “Near-field radiative heat transfer between two plane surfaces with one having a dielectric coating,” *Journal of Quantitative Spectroscopy and Radiative Transfer* **110**, 1027 – 1036 (2009).
- [8] V. B. Svetovoy, P. J. van Zwol, and J. Chevrier, “Plasmon enhanced near-field radiative heat transfer for graphene covered dielectrics,” *Phys. Rev. B* **85**, 155418 (2012).
- [9] P. J. van Zwol, K. Joulain, P. Ben Abdallah, J. J. Greffet, and J. Chevrier, “Fast nanoscale heat-flux modulation with phase-change materials,” *Phys. Rev. B* **83**, 201404 (2011).
- [10] P. J. van Zwol, L. Ranno, and J. Chevrier, “Tuning near field radiative heat flux through surface excitations with a metal insulator transition,” *Phys. Rev. Lett.* **108**, 234301 (2012).
- [11] Y. Yang, S. Basu, and L. Wang, “Radiation-based near-field thermal rectification with phase transition materials,” *Applied Physics Letters* **103**, 163101 (2013).
- [12] S.-A. Biehs, P. Ben-Abdallah, F. S. S. Rosa, K. Joulain, and J.-J. Greffet, “Nanoscale heat flux between nanoporous materials,” *Opt. Express* **19**, A1088–A1103 (2011).
- [13] R. Esquivel-Sirvent, “Ultra thin metallic coatings to control near field radiative heat transfer,” *AIP Advances* **6**, 095214 (2016), <http://dx.doi.org/10.1063/1.4963297>.
- [14] E. Y. Santiago, J. E. Pérez-Rodríguez, and R. Esquivel-Sirvent, “Dispersive properties of mesoporous gold: van der waals and near-field radiative heat interactions,” *The Journal of Physical Chemistry C* **0**, null (0), <http://dx.doi.org/10.1021/acs.jpcc.7b02894>.
- [15] S. Basu, Y. Yang, and L. Wang, “Near-field radiative heat transfer between metamaterials coated with silicon carbide thin films,” *Applied Physics Letters* **106**, 033106 (2015).
- [16] S. Basu and Z. M. Zhang, “Ultrascale penetration depth in nanoscale thermal radiation,” *Applied Physics Letters* **95**, 133104 (2009), <http://dx.doi.org/10.1063/1.3238315>.
- [17] E. Moncada-Villa, V. Fernández-Hurtado, F. J. García-Vidal, A. García-Martín, and J. C. Cuevas, “Magnetic field control of near-field radiative heat transfer and the realization of highly tunable hyperbolic thermal emitters,” *Phys. Rev. B* **92**, 125418 (2015).
- [18] V. Fernández-Hurtado, F. J. García-Vidal, S. Fan, and J. C. Cuevas, “Enhancing near-field radiative heat transfer with si-based metasurfaces,” *Phys. Rev. Lett.* **118**, 203901 (2017).
- [19] C.M Hargreaves, “Anomalous radiative transfer between closely-spaced bodies,” *Physics Letters A* **30**, 491 – 492 (1969).
- [20] D. Polder and M. Van Hove, “Theory of radiative heat transfer between closely spaced bodies,” *Phys. Rev. B* **4**, 3303–3314 (1971).
- [21] B. Song, A. Fiorino, E. Meyhofer, and P. Reddy, “Near-field radiative thermal transport: From theory to experiment,” *AIP Advances* **5**, 053503 (2015).
- [22] Andrew C. Jones, Brian T. O’Callahan, H. U. Yang, and M. B. Raschke, “The thermal near-field: Coherence, spectroscopy, heat-transfer, and optical forces,” *Progress in Surface Science* **88**, 349 – 392 (2013).
- [23] R. Hillenbrand, T. Taubner, and F. Keilmann, “Phonon-enhanced light-matter interaction at the nanometre scale,” *Nature* **418**, 159–162 (2002).
- [24] F. Huth, M. Schnell, J. Wittborn, N. Ocelic, and R. Hillenbrand, “Infrared-spectroscopic nanoimaging with a thermal source,” *Nat. mat.* **10**, 352–356 (2011).

- [25] Y. De Wilde, F. Formanek, R. Carminati, B. Gralak, P.-A. Lemoine, K. Joulain, J.-P. Mulet, Y. Chen, and J.-J. Greffet, “Thermal radiation scanning tunnelling microscopy,” *Nature* **444**, 740–743 (2006).
- [26] A. Kittel, W. Müller-Hirsch, J. Parisi, S.-A. Biehs, D. Reddig, and M. Holthaus, “Near-field heat transfer in a scanning thermal microscope,” *Phys. Rev. Lett.* **95**, 224301 (2005).
- [27] E. Rousseau, A. Siria, G. Jourdan, S. Volz, F. Comin, J. Chevrier, and J.-J. Greffet, “Radiative heat transfer at the nanoscale,” *Nat Photon* **3**, 514–517 (2009).
- [28] R. St-Gelais, L. Zhu, S. Fan, and M. Lipson, “Near-field radiative heat transfer between parallel structures in the deep subwavelength regime,” *Nat. Nanotech* **11**, 515–519 (2016).
- [29] M. Francoeur, “Near-field radiative energy transfer: Nanostructures feel the heat,” *Nat Nano* **10**, 206–208 (2015).
- [30] B. Song, Y. Ganjeh, S. Sadat, D. Thompson, A. Fiorino, V. Fernández-Hurtado, J. Feist, F. J. Garcia-Vidal, J. C. Cuevas, P. Reddy, and E. Meyhofer, “Enhancement of near-field radiative heat transfer using polar dielectric thin films,” *Nat Nano* **10**, 253–258 (2015).
- [31] B. Song, D. Thompson, A. Fiorino, Y. Ganjeh, P. Reddy, and E. Meyhofer, “Radiative heat conductances between dielectric and metallic parallel plates with nanoscale gaps,” *Nat. Nanotech.* **11**, 509–514 (2016).
- [32] K. Kloppstech, N. Konne, S. Biehs, A. W. Rodriguez, L. Worbes, D. Hellmann, and A. Kittel, “Giant heat transfer in the crossover regime between conduction and radiation,” *Nat. Comm.* **8**, 14475 (2017).
- [33] K. Joulain, J.-P. Mulet, F. Marquier, R. Carminati, and J.-J. Greffet, “Surface electromagnetic waves thermally excited: Radiative heat transfer, coherence properties and casimir forces revisited in the near field,” *Surface Science Reports* **57**, 59 – 112 (2005).
- [34] P. Ben-Abdallah, K. Joulain, J. Drevillon, and G. Domingues, “Near-field heat transfer mediated by surface wave hybridization between two films,” *J. Appl. Phys.* **106**, 044306 (2009).
- [35] X. L. Liu, T. J. Bright, and Z. M. Zhang, “Application conditions of effective medium theory in near-field radiative heat transfer between multilayered metamaterials,” *Journal of Heat Transfer* **136**, 092703–092703 (2014).
- [36] R. Messina, M. Antezza, and P. Ben-Abdallah, “Three-body amplification of photon heat tunneling,” *Phys. Rev. Lett.* **109**, 244302 (2012).
- [37] M. Aspelmeyer, T. J. Kippenberg, and F. Marquardt, “Cavity optomechanics,” *Rev. Mod. Phys.* **86**, 1391–1452 (2014).
- [38] U. Fano, “Effects of configuration interaction on intensities and phase shifts,” *Phys. Rev.* **124**, 1866–1878 (1961).
- [39] B. Luk’yanchuk, N. I. Zheludev, S. A. Maier, N. J. Halas, P. Nordlander, H. Giessen, and C. T. Chong, “The fano resonance in plasmonic nanostructures and metamaterials,” *Nat Mater* **9**, 707–715 (2010).
- [40] A. E. Miroshnichenko, S. Flach, and Y. S. Kivshar, “Fano resonances in nanoscale structures,” *Rev. Mod. Phys.* **82**, 2257–2298 (2010).
- [41] N. Liu, L. Langguth, T. Weiss, J. Kastel, M. Fleischhauer, T. Pfau, and H. Giessen, “Plasmonic analogue of electromagnetically induced transparency at the drude damping limit,” *Nat. Mat.* **8**, 758–762 (2009).
- [42] S. R. K. Rodriguez, Y. T. Chen, T. P. Steinbusch, M. A. Verschuuren, A. F. Koenderink, and J. Gómez Rivas, “From weak to strong coupling of localized surface plasmons to guided modes in a luminescent slab,” *Phys. Rev. B* **90**, 235406 (2014).
- [43] E. A. Vinogradov and I. A. Dorofeev, “Thermally stimulated electromagnetic fields of solids,” *Physics-Uspekhi* **52**, 425 (2009).
- [44] R. Esquivel, C. Villarreal, and W. L. Mochán, “Exact surface impedance formulation of the casimir force: Application to spatially dispersive metals,” *Phys. Rev. A* **68**, 052103 (2003).
- [45] R. Márquez-Islas, B. Zenteno-Mateo, B. Flores-Desirena, A. Reyes-Coronado, and F. Pérez-Rodríguez, “Plasmaphoton polaritons in superlattices of semimetal bismuth and polaritonic material,” *Opt. Mater. Express* **5**, 2820–2834 (2015).
- [46] J. Toudert, R. Serna, I. Camps, J. Wojcik, P. Mascher, E. Rebollar, and T. A. Ezquerra, “Unveiling the far infrared-to-ultraviolet optical properties of bismuth for applications in plasmonics and nanophotonics,” *The Journal of Physical Chemistry C* **121**, 3511–3521 (2017), <http://dx.doi.org/10.1021/acs.jpcc.6b10331>.
- [47] A. I. Maarroof, M. B. Cortie, and G. B. Smith, “Optical properties of mesoporous gold films,” *Journal of Optics A: Pure and Applied Optics* **7**, 303 (2005).
- [48] A. I. Maarroof, A. Gentle, G. B. Smith, and M. B. Cortie, “Bulk and surface plasmons in highly nanoporous gold films,” *Journal of Physics D: Applied Physics* **40**, 5675 (2007).
- [49] C. L. C. Smith, N. Stenger, A. Kristensen, N. A. Mortensen, and S. I. Bozhevolnyi, “Gap and channeled plasmons in tapered grooves: a review,” *Nanoscale* **7**, 9355–9386 (2015).
- [50] See Supplemental Material at [URL will be inserted by publisher] for calculations of the NFRHT in a cavity made by porous Bi, semi infinite Bi, semi infinite NaBr, G-SPP dispersion relation and total spectral heat flux.
- [51] K. J. Boller, A. Imamoglu, and S. E. Harris, “Observation of electromagnetically induced transparency,” *Phys. Rev. Lett.* **66**, 2593–2596 (1991).
- [52] M. Fleischhauer, A. Imamoglu, and J. P. Marangos, “Electromagnetically induced transparency: Optics in coherent media,” *Rev. Mod. Phys.* **77**, 633–673 (2005).
- [53] S. Zhang, D. A. Genov, Y. Wang, M. Liu, and X. Zhang, “Plasmon-induced transparency in metamaterials,” *Phys. Rev. Lett.* **101**, 047401 (2008).
- [54] P. Tassin, L. Zhang, Th. Koschny, E. N. Economou, and C. M. Soukoulis, “Low-loss metamaterials based on classical electromagnetically induced transparency,” *Phys. Rev. Lett.* **102**, 053901 (2009).
- [55] P. Tassin, L. Zhang, R. Zhao, A. Jain, T. Koschny, and C. M. Soukoulis, “Electromagnetically induced transparency and absorption in metamaterials: The radiating two-oscillator model and its experimental confirmation,” *Phys. Rev. Lett.* **109**, 187401 (2012).